



# Experimental and Numerical Analysis Over Power Series Nose Cone

Vineet Kumar Rathi

**Abstract:** While designing aerospace vehicles, one of the most important factors to consider is drag. Drag force opposes the vehicle and causes it to slow down, which in turn requires more fuel to maintain flight. The vehicle nose cone plays a vital role in minimizing the drag during flight. The shape of the vehicle's body, as well as the fluid characteristics and orientation, can all have a significant impact on drag. To determine the most effective nose cone design, a study was conducted to test the aerodynamic performance of power series nose cone profiles using both experimental and computational techniques. All nose cone profiles with the same L/D ratio were assessed at 25 m/s speed with no angle of attack. The experimental data, including pressure, velocity, and drag, were then compared with computational data to ensure the accuracy of the wind tunnel experiments. The primary factor in determining the best shape for the subsonic flow range among all the nose cone profiles was the drag coefficient. The nose cone with a power of 0.25 was found to have the lowest drag coefficient at low subsonic speeds, making it the best-performing nose cone profile among those investigated. During take-off, drag is the most undesirable factor, as it can significantly impact the fuel efficiency of the vehicle. Therefore, it is crucial to have the least amount of drag possible. In this case, the nose cone with a power of 0.25 can be used in the initial stages of the rocket to minimize drag and maximize fuel efficiency.

**Keywords:** Nose Cones, CFD, Aerodynamics Analysis, Coefficient of Drag, Pressure

## NOMENCLATURE

g	Gravity acceleration
$\rho_w$	Water density, $\text{kg/m}^3$
$\rho_a$	Air density, $\text{kg/m}^3$
$\Delta H$	Pressure head
$V_\infty$	Inlet velocity, m/s

## I. INTRODUCTION

Rocket design takes into account several forces that affect both fuel efficiency and flight profile during a rocket's flight. One of these forces is the drag force, which is divided into two types - wave drag and skin friction drag. Drag is undesirable during flight as it slows down the rocket, requiring more fuel to reach the same altitude. Therefore, while designing the exterior part of the rocket, the primary goal is to minimize drag force. Forebody wave drag is caused by the nose cone, so the nose cone is designed to reduce drag forces during flight.

Manuscript received on 30 January 2024 | Revised Manuscript received on 07 February 2024 | Manuscript Accepted on 15 February 2024 | Manuscript published on 28 February 2024.

\*Correspondence Author(s)

Vineet Kumar Rathi\*, Junior Research Fellow, Department of Mechanical Science, Indian Institute of Technology, Goa, India. E-mail: [Vinetrathi4200@gmail.com](mailto:Vinetrathi4200@gmail.com), ORCID ID: [0000-0002-9682-931X](https://orcid.org/0000-0002-9682-931X)

© The Authors. Published by Blue Eyes Intelligence Engineering and Sciences Publication (BEIESP). This is an [open access](https://creativecommons.org/licenses/by-nc-nd/4.0/) article under the CC-BY-NC-ND license <http://creativecommons.org/licenses/by-nc-nd/4.0/>

Various factors affect drag, including body shape, fluid characteristics, and body orientation in the fluid [1][13][14][15]. Modern rockets and missiles use different nose cone shapes, such as conical, power series, tangent & secant ogive, etc. These nose cones are identified by their characteristic equation, which describes the curvature they follow. Any aerodynamic design issue involves identifying the body's geometry with the lowest drag coefficient (Cd). The nose cone's geometry has a significant impact on an object's aerodynamic properties. People have debated the nose cone's form for over a century, and its geometry affects the object's penetration and aerodynamic drag. In both cases, the pressure distribution over the body was described using Newton's theory. However, the resultant forms' closeness pointed to a significant relationship between aerodynamic drag and the mechanics of shape penetration. Rosy Subha et al. [2] and his team conducted a study using numerical analysis to compare the aerodynamic characteristics of different nose cone profiles. They aimed to identify a profile that exhibited a low coefficient of pressure and a high critical Mach number. The researchers used ANSYS software to analyze the data and concluded that the Von Karman Ogive model was the most superior among the four profiles. This model displayed better aerodynamic qualities, with a higher critical Mach number and lower pressure coefficient, particularly under subsonic conditions.

Yeshwanth et al. [3] aimed to optimize nose cone design for avionics, studying various shapes using CFD simulations at subsonic speeds. They found that elliptical nose cones showed the lowest drag coefficients at Mach 0.4, 0.6, and 0.8, while the parabolic shape exhibited higher drag coefficients at these speeds. These findings hold promise for enhancing aerodynamic performance in avionic design. Kiran Kumar et al. [4] conducted a study to compare the effectiveness of two different models of nose cones i.e. Conical and Ogive with the same payload capacity. Velocity, pressure and other parameters at various Mach numbers were examined using ANSYS FLUENT. The tangent ogive nose cone showed the lowest drag coefficient and high-velocity reduction at edges compared to the other one [17]. Rozario et al. [5] studied the aerodynamic characteristics of different nose cone shapes at higher Mach numbers. The shapes analyzed included the bi-cone, ogive, and spherical-blunt cone. The study utilized theoretical, experimental, and CFD methods to compare the aerodynamic performance of each shape. The findings revealed that the ogive-shaped nose cone had better aerodynamic characteristics compared to the other-shaped nose cone. The bi-cone model exhibited the minimum static pressure value, while the spherical blunted model had the maximum static pressure value.

## Experimental and Numerical Analysis Over Power Series Nose Cone

The ogive nose cone had the highest pressure coefficient, whereas the spherically blunt cone had the lowest pressure coefficient. In 2015, Schinetsky et al. [6] proposed a method for selecting the most optimal shape of a nose. This approach involved constructing the various components of the shape while simultaneously minimizing aerodynamic wave drag. The research also examined ways to reduce aerodynamic wave drag through analytical means. The results indicated that an ideal shape conforms to a two-thirds power law. Foster et al. [7] performed research to contrast and evaluate the effectiveness of two approaches for optimising the geometry of the nose cone: hybrid gradient optimisation and hybrid genetic optimisation. These techniques were used to assess the best forms at an attack angle of 0 degrees. Deepak et al. [8] employed the multipoint response surface design methodology to craft an optimal nose cone shape, taking into account aerodynamic drag, heat dissipation, and payload capacity. Like that, blunt forms were produced using the ANSYS CFX computational fluid dynamics solver, an evolutionary algorithm optimisation technique, and the particle swarm optimisation approach. The optimised form also used a spherically rounded tip and reduced drag by 2%.

### A. Types of Nose Cone

Depending on the vehicle's speed and purpose, a certain style of nose cone is used. Because of this, there are many distinct nose cone profiles available, including the Conical, Parabolic, Elliptical, Haack series, and Power series nose cones. The parameters governing the nose cone geometry are given in Table 1 and shown in Fig. 1.

**Table 1: Nose Cone Geometry Parameters**

<i>L</i>	Total length
<i>R</i>	Base radius
<i>y</i>	Radius at any point from 0 to <i>L</i>
<i>C/L</i>	The profile is rotated around the centreline to create the nose cone's entire body of rotation.

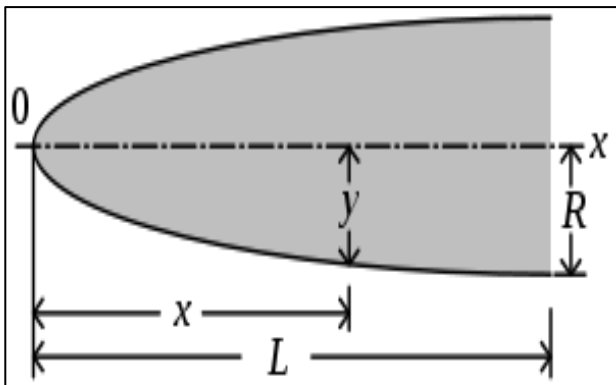


**Fig. 1. Nose Cone Nomenclature**

#### a. Power Series Nose Cone

Ranjan et al. [9][16] make an effort to improve the efficiency of aircraft by designing various nose cone profiles. Parabolic, cone, and flat-face cylinder are the shapes that come under the category of power series nose cone. The nose cone shape bluntness is defined by *P* power. The tip of the cone changes from sharp to blunt as the value of *n* changes from 1 to 0 as shown in Fig. 2. Four types of power are being taken i.e., 0.25, 0.5, 0.75, and 1.

For, *P* = 1 conical nose cone

*P* = 0.5 true parabola

*P* = 0 cylindrical body

Governing equation:

$$Y = \frac{D}{2} * \left(1 - \frac{X}{L}\right)^P \quad (1)$$

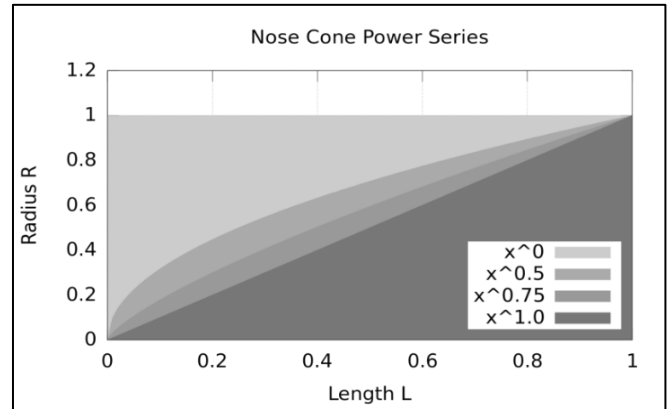


**Fig. 2. Curves for a Different Power of Nose Cone [8]**

### B. Nose Cone Drag Characteristics

At speeds below Mach 0.8, the nose cone doesn't contribute much to the drag acting on a body. Instead, the primary factor is friction drag, which depends on the surface area that comes into contact with the air, the smoothness of the surface, and any imperfections in the shape. For model rockets that fly at subsonic speeds, a short, blunt, and smooth elliptical shape is typically the best choice. However, as the speed increases and approaches the transonic range, the shape of the nose cone becomes increasingly important in determining the amount of drag. Garry A. Crowell Sr [10] identified the basic shape of the nose cone, the fineness ratio, and the bluntness ratio as the main factors affecting pressure drag.

**Wetted Area** - The overall surface area of the nose cone that is in touch with the fluid may be thought of as its definition. The wetted area does not include the nose cone's base. Additionally, the overall amount of wetted area directly affects the friction drag pressing on the body. The value of the wetted area is essential for calculating drag.

For conical:

$$A_{wet} = \pi R + \sqrt{R^2 + L^2} \quad (2)$$

**General Shape** - Various studies show drag characteristics based on nose cone profiles at different Mach numbers. Fig. 3 compiles data of how well the different nose cone profiles behave at different Mach numbers as well as estimates at what Mach number they are the most efficient. Rankings are in the following order: Excellent (1), Good (2), Fair (3), and Below Average (4).

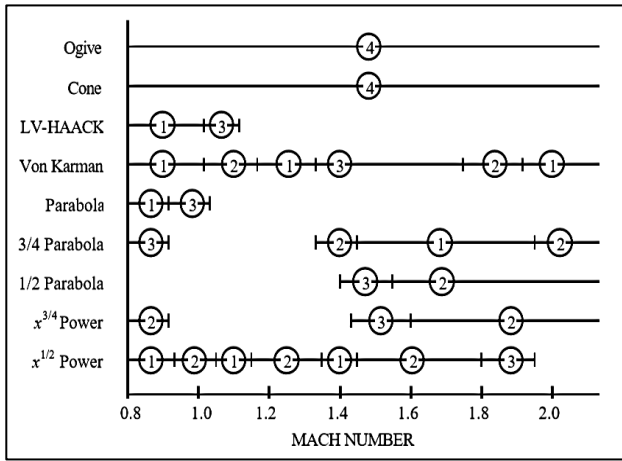


**Fig. 3. Comparison of the Transonic-to-Low Mach Regions' Drag Properties for Different Types of Nose Cone Shapes [9]**

**Fineness ratio** - The term "Fineness Ratio," often referred to as "Aspect Ratio," refers to the relationship between a nose cone's length and base diameter. At supersonic speeds, wave drag was affected by the fineness ratio. The wetted area rises with an increase in fineness ratio, which also increases the skin friction drag, which is computed using the formula below:

$$A_R = \frac{L}{2R} \quad (3)$$

**C. Effect of Different Nose Cone Profiles on Boundary Layer Separation**

Varma et al. [11] determined the aerodynamic properties of several nose cone designs with the critical Mach number and pressure coefficient. The CFD study was done with a fineness ratio of 6 for several nose cone profiles, including parabolic, ogives, conical, and von Karman ogive. The main objective was to study whether Boundary layer separation can be delayed by using different shapes of nose cones. The assumption was to get large static pressure at the base of the forebody because large static pressure at the base gives a high critical Mach number and the least adverse pressure. To find out which nose cone shape gives the highest critical Mach number along with minimum pressure coefficient CFD analysis was carried out on ANSYS software. The inlet condition was set to 0.8 Mach and meshing was done with a Hybrid grid around the Nose cone along with an unstructured grid with 0.4 million tetrahedral cells element. Turbulent model SST with convergence criteria of  $10^{-4}$  was used. It was found that the flow is slowly speeding on the Von Karman profile resulting in a higher critical Mach number along with a minimum coefficient of pressure. Both are desirable conditions for subsonic flow.

CFD analysis was performed by Harish et al. [12] on a parabolic series nose cone to find out the distribution of surface base pressure. In their investigation, they selected four parabolic series profiles with fineness ratios of 2.75: ¼ parabola, ½ parabola, ¾ parabola & complete parabola. Using ANSYS ICEM CF 15.0, the four profiles' flow was computationally analysed. For simulation, the Shear Stress K-Turbulence Model was used. The study also analysed the impact of nose cone shape on the drag coefficient and surface & base pressure coefficient. The findings revealed that the

fully parabolic nose cone exhibited superior pressure distribution compared to the previous parabolic nose cone series. Additionally, it demonstrated a reduced drag coefficient

**II. EXPERIMENTAL PROCEDURE**

**A. Nose Cone Design**

The arithmetic operations were utilized along with Eq. 1 to define the curve along the axis using MS Excel. The length of the nose cone was taken as 117mm after scaling down an Honest John rocket to the ratio of 20:1. That is x varies from 0 to 117 mm. The above equation was entered into Excel and the graph for various nose cones was obtained as illustrated in Fig. 4. The coordinates of these nose cones have been mentioned in Annexures A, B, C and D for power 1, 0.75, 0.5, 0.25 nose cone, respectively.

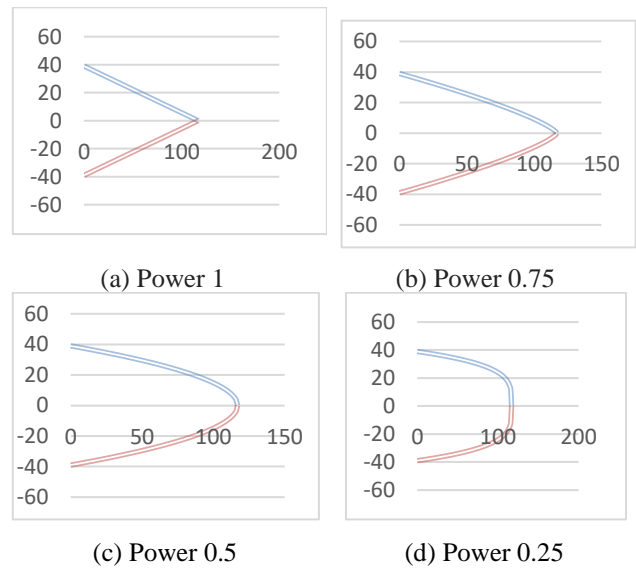
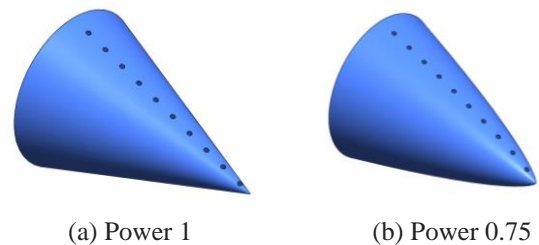


**Fig. 4. Curve for Power Series Nose Cone**

**B. Three-Dimensional Modelling**

After plotting the graphs in Excel, the above-given curves were then imported to SOLIDWORKS to create 3D CAD models. Along with the nose cone, another assembly was also designed in SOLIDWORKS to mount the nose cone in the wind tunnel. A CAD model of the power series nose cone is given in Fig. 5.



## Experimental and Numerical Analysis Over Power Series Nose Cone

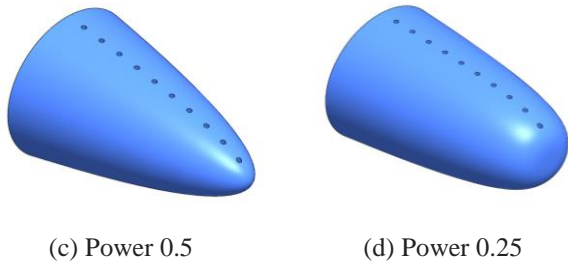


Fig. 5. CAD Model of Power Series Nose Cone

### C. Fabrication

Creator Pro 3D was used to print the following CAD files. The Fused Deposition Modelling (FDM) technique serves as the printer's foundation. With the highest precision and reproducibility of any 3D printing process, this technology is used to create parts that are robust, long-lasting, and stable in terms of their dimensions. These cones were printed in three dimensions using polylactic acid (PLA). It is a thermoplastic aliphatic polyester that is both biodegradable and bioactive. PLA is often made from renewable biomass, such as corn, cassava, sugarcane, or sugar beetroot pulp, which has been fermented with plant starch. Each of the nose cones took roughly four hours to produce on average. The fabricated nose cone is shown in Fig. 6. The properties of PLA material are given in Table 2.

Table 2: Material Properties of Polylactic Acid (PLA)

Melt Temperature	145 – 160°C
Glass transition temperature	~ 60°C
Melt volume rate	6.73 cm <sup>3</sup> /10min
Melt flow rate	6.09 g/10min
Density	1.26 g/cm <sup>3</sup>
Odour	Odourless
Solubility	Insoluble in water



Fig. 6. Fabricated 3D Models

### D. Validation of Experimental Setup

The Pressure coefficient ( $C_p$ ) estimated for a cylinder was investigated at different angles of attack and the data obtained was then compared with theoretical data to confirm the experimental setup to perform experimental analysis. The intake velocity was also calculated using wind tunnel calibration. Given below are the formulae that were used to calculate the parameters. Velocity calculations were done by using the following formula.

$$C_p = 1 - \left(\frac{v}{V_\infty}\right)^2 \quad (4)$$

Rearranging the terms, we get

$$V = V_\infty \sqrt{1 - C_p} \quad (5)$$

Pressure calculations were done from the following formula.

$$C_p = \frac{(P - P_\infty)}{\frac{1}{2} \rho v^2} \quad (6)$$

### E. Computational Analysis

ANSYS FLUENT was used to provide a numerical solution. The geometry and domain were made, and a grid independence test was done with different numbers of nodes on the domain. After finalizing the number of elements taken in meshing the setup was created to analyse aerodynamic parameters on the nose cone.

### F. Domain

The domain was taken after various analyses in ANSYS FLUENT. The parameters selected for the domain for all the power series nose cones are shown in Table 3 and the geometry is shown in Fig. 7.

Table 3: Power Series Nose Cone Domain Parameters

The radius of the domain (mm)	Length of model (mm)	The base diameter of the model (mm)
585	117	78

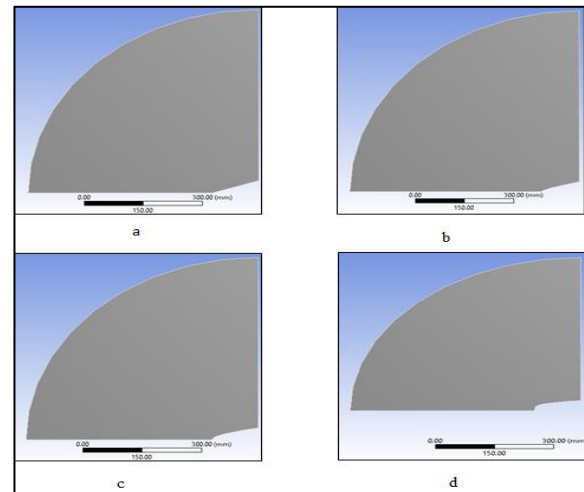


Fig. 7. Nose Cone Geometry. (a) Power 1, (b) Power 0.75, (c) Power 0.5, (d) Power 0.25

### G. Grid Independency Test

Computational grids for nose cones with constant fineness ratio were constructed using the meshing tool of ANSYS CFD to observe the aerodynamic parameters after the encountered incoming airflow. Structured grids consisting of precisely quadrilateral cells were created with varying divisions from 200 to 300 nodes, with increments of 25 nodes in each division.

Since the accuracy of results was highly dependent on the quality of the mesh in the proximity of the solid body in the airflow; a dense mesh near the nose cone was constructed to effectively capture the airflow/body interactions. A bias factor i.e., the largest to the smallest edge, of 20 on the inlet curve proved to be optimum allowing the construction of a dense mesh near the body and a coarse mesh where the airflow effects were negligible. To ensure that the aerodynamic characteristics were independent of the size of the grid that was constructed, a grid independence test was performed. The number of divisions on each edge were varied as 200, 225, 250, 275, 300, and 325. The aerodynamic parameters were then obtained and compared while keeping the rest of the airflow parameters like observing the percentage improvement in accuracy of the results exclusively due to refinement of the constructed grid. To conduct the grid independence test, the total drag force that a conical nose cone with a finesse ratio of 3 encountered in the airflow was considered and compared. The coefficient of drag was taken as a key parameter and variation was taken by increasing the number of nodes by 25. It was observed that the coefficient of drag was increasing, and the difference was much less between 275, 300 and 325 nodes as shown in Fig. 8. So, a grid with 275 nodes was selected for further analysis on nose cones. The named selection for the selected domain is shown in Fig. 9.

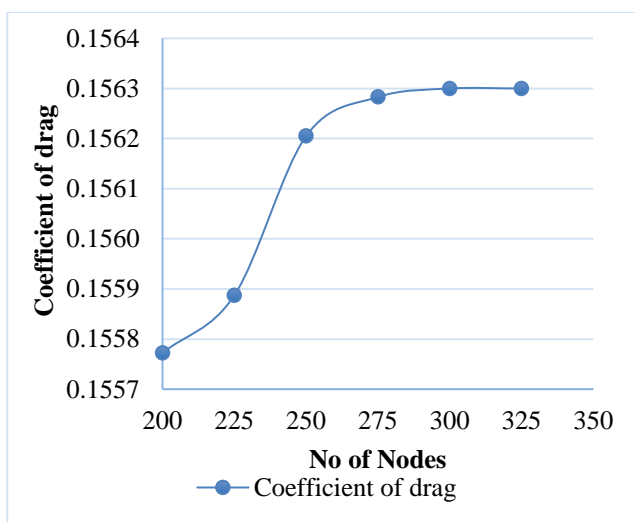


Fig. 8. Grid Independence Test Result

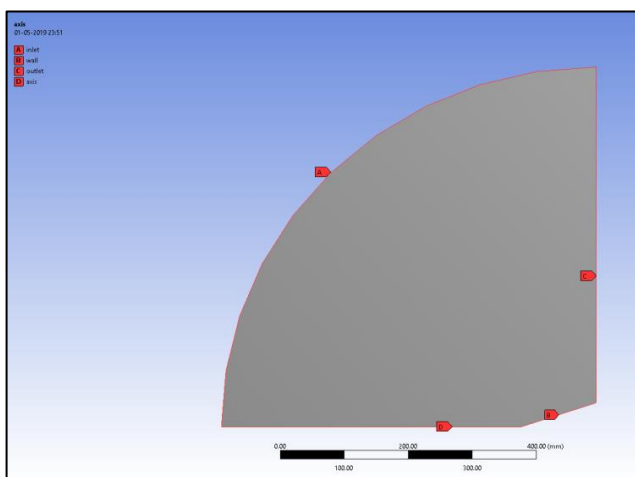


Fig. 9. Name Selection on the Conical Nose Cone

H. Meshing

The process of creating a quadrilateral mesh that closely resembles a geometric domain is known as mesh generation. The phrase "grid generation" is frequently used synonymously. The mesh has an impact on the computational time's precision, convergence, and speed. The geometry was used as shown in Fig. 10 and mesh control in Fig. 11.

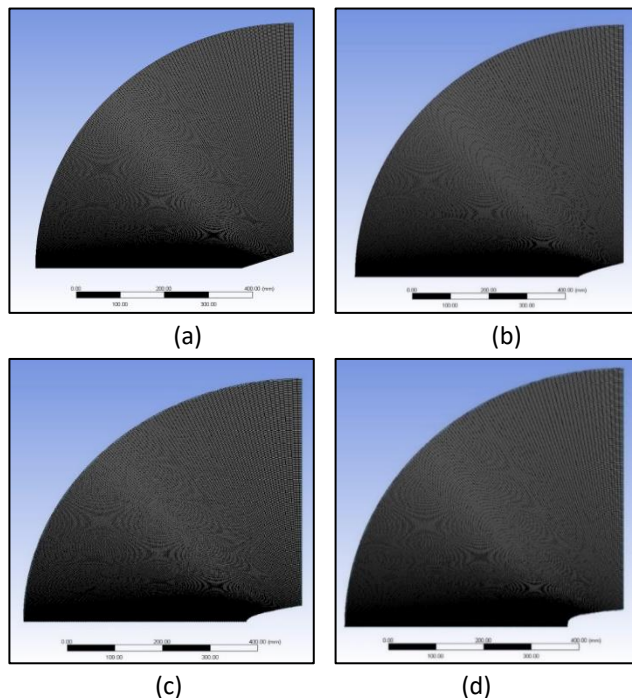


Fig. 10. Meshing, (a) Power 1, (b) Power 0.75, (c) Power 0.5, (d) Power 0.25

Object Name	Edge Sizing	Edge Sizing 2	Face Meshing
State	Fully Defined		
<b>Scope</b>			
Scoping Method	Geometry Selection		
Geometry	2 Edges	1 Face	
<b>Definition</b>			
Suppressed	No		
Type	Number of Divisions		
Number of Divisions	275	300	
Behavior	Hard		
Bias Type	No Bias		
Bias Option	Bias Factor		
Bias Factor	20.		
Reverse Bias	No Selection		
Mapped Mesh			Yes
Method	Quadrilaterals		
Constrain Boundary	No		
<b>Advanced</b>			
Specified Sides	No Selection		
Specified Corners	No Selection		
Specified Ends	No Selection		

Fig. 11. Mesh Control

**I. Boundary Conditions and Physics Setup**

A steady, inviscid, and dimension-based pressure solver was utilized to conduct axisymmetric simulations on the airflow's interaction with the body and predict key aerodynamic phenomena for airflow through a power series nose cone. The simulations were performed using the K-SST turbulence model, with air flowing at a velocity of 25 m/s and zero-degree angle of attack over the power series nose cones.

**J. Computational Data**

The examination of the power series nose cone yielded the following variables: fluctuation in velocity, static pressure, dynamic pressure, total drag coefficient, and skin friction drag on model surfaces. By using the ANSYS tool data was obtained along the curve length of each model. The interpolation method was used to get the values at specific points in the model.

**K. Experimental Analysis**

In the experimental study, the following parameters were obtained for each of the models (power 1, 0.75, 0.5, 0.25) such as velocity, static pressure, dynamic pressure, total drag coefficient and skin friction drag. Using the data obtained from the experimental study of the models various graphs were plotted. The models were placed in a wind tunnel and the respective tubes were attached to the multi-tube manometer to obtain the pressure head. By utilizing the respective values of  $\Delta h$  dynamic pressure along the surface models was obtained. Fig. 12 shows the power series nose cone placed in the test section of a wind tunnel.

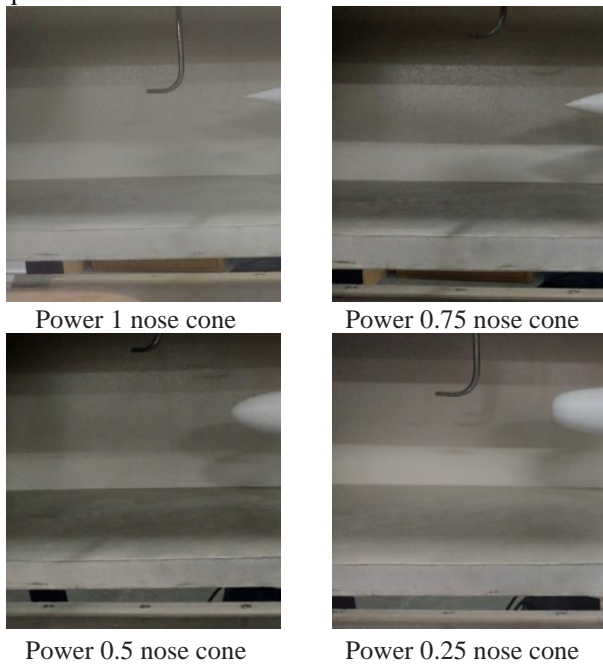


Fig. 12. Nose Cones Placed in the Test Section of the Wind Tunnel

**III. RESULT AND DISCUSSION**

**A. Numerical Analysis Results**

a. *Static and Dynamic Pressure Variations Over the Length of The Curve*

**Power 1 Nose Cone:** The change in static and dynamic pressure over the length of the curve and the contours of both pressures are shown in Fig. 13 and 14 respectively.

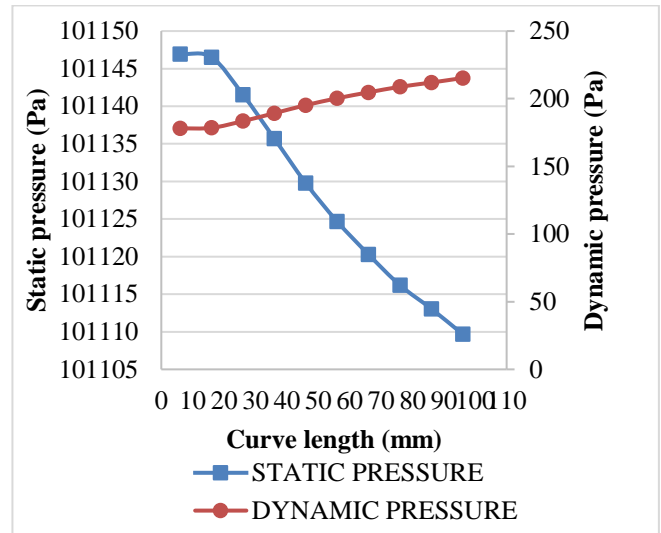


Fig. 13. Static and Dynamic Pressure Variation of Power 1 Nose Cone

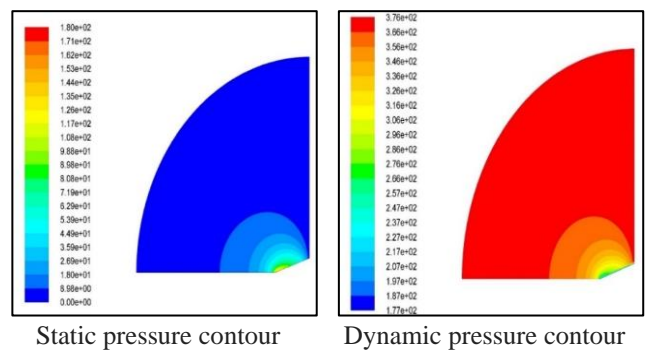


Fig. 14. Pressure Contour of Power 1 Nose Cone

**Power 0.75 Nose Cone:** The change in static and dynamic pressure over the length of the curve and the contours of both pressures are shown in Fig. 15 and 16 respectively.

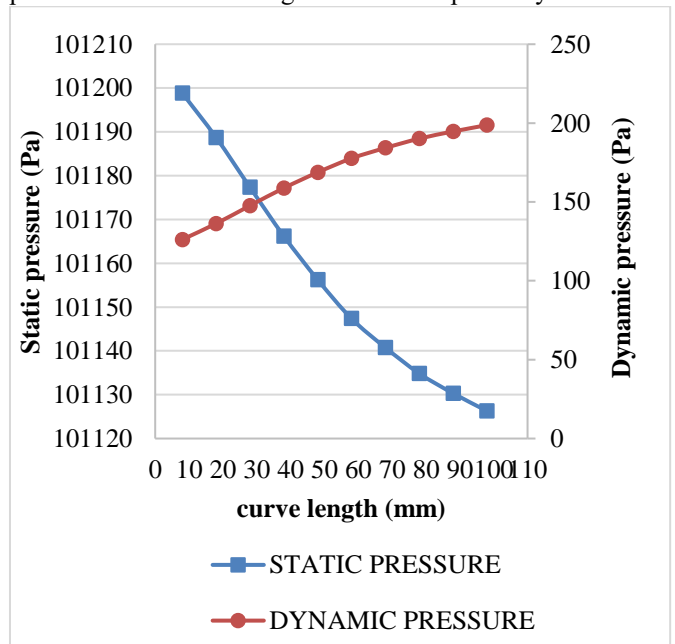
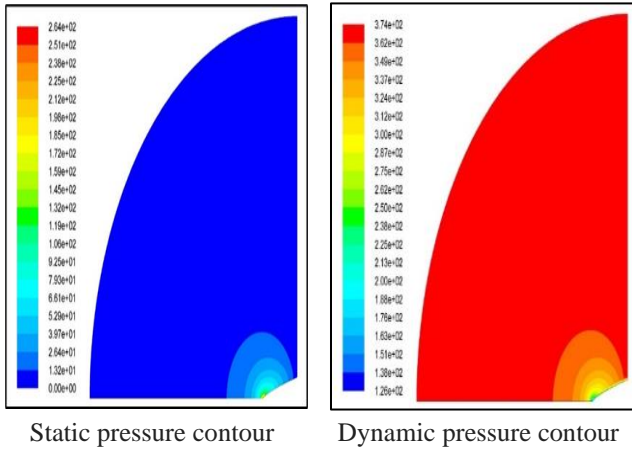


Fig. 15. Static and Dynamic Pressure Variation of Power 0.75 Nose Cone



Static pressure contour      Dynamic pressure contour

**Fig. 16. Pressure Contour of Power 0.75 Nose Cone**

**Power 0.5 Nose Cone:** The change in static and dynamic pressure over the length of the curve and the contours of both pressures are shown in Fig. 17 and 18 respectively.

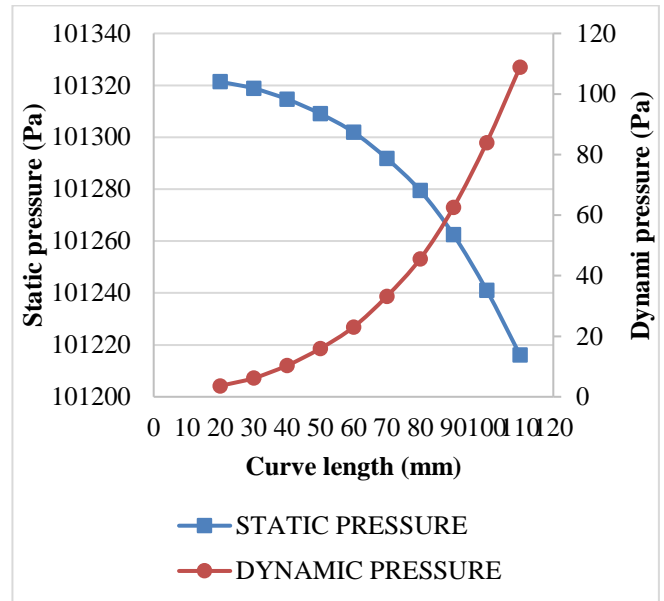


**Fig. 19. Static and Dynamic Pressure Variation of Power 0.25 Nose Cone**

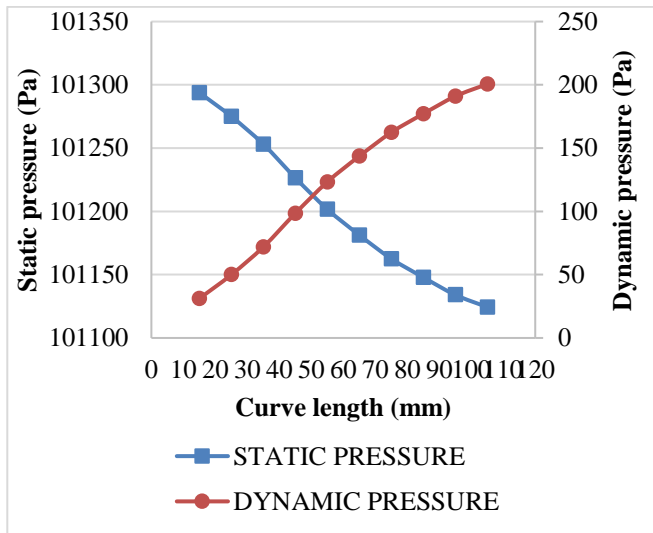
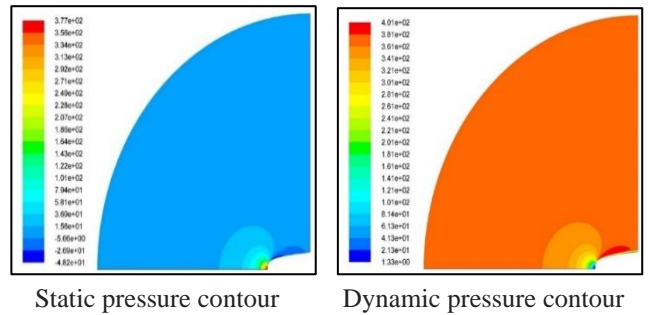


**Fig.17. Static and Dynamic Pressure Variation of Power 0.5 Nose Cone**

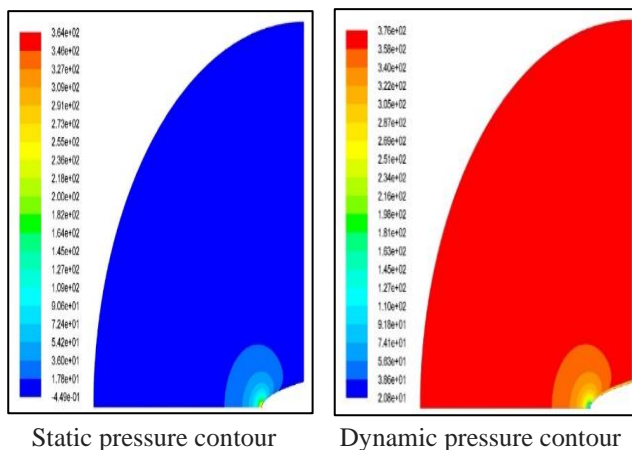


Static pressure contour      Dynamic pressure contour

**Fig. 20. Pressure Contour of Power 0.25 Nose Cone**

*b. Vector Contours*

The vector controls are used to determine whether a vortex is present on the profile's surface. The velocity vectors for the power 1, 0.75, 0.5, and 0.25 nose cones are shown in Fig. 21.



Static pressure contour      Dynamic pressure contour

**Fig. 18. Pressure Contour of Power 0.5 Nose Cone**

**Power 0.25 Nose Cone:** The change in static and dynamic pressure over the length of the curve and the contours of both pressures are shown in Fig. 19 and 20 respectively.

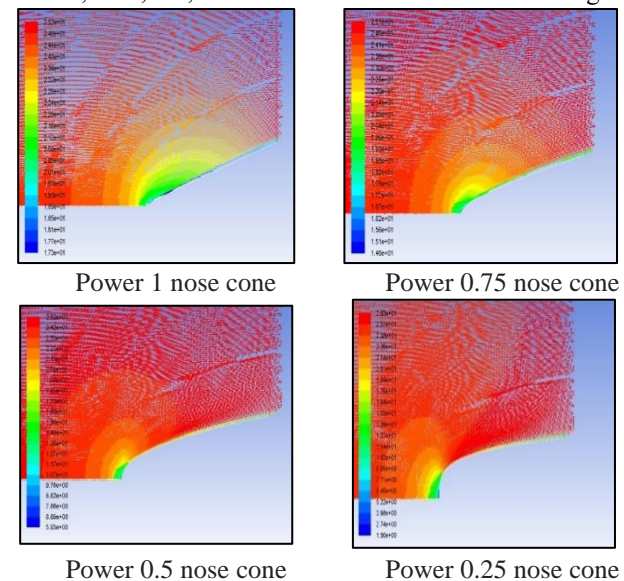


**Fig. 21. Vector Contours of Power Series Nose Cones**

c. *Turbulence Viscosity Contour*

Fig. 22 represents the turbulence viscosity contour of power 1, 0.75, 0.5 and 0.25 nose cone, respectively.

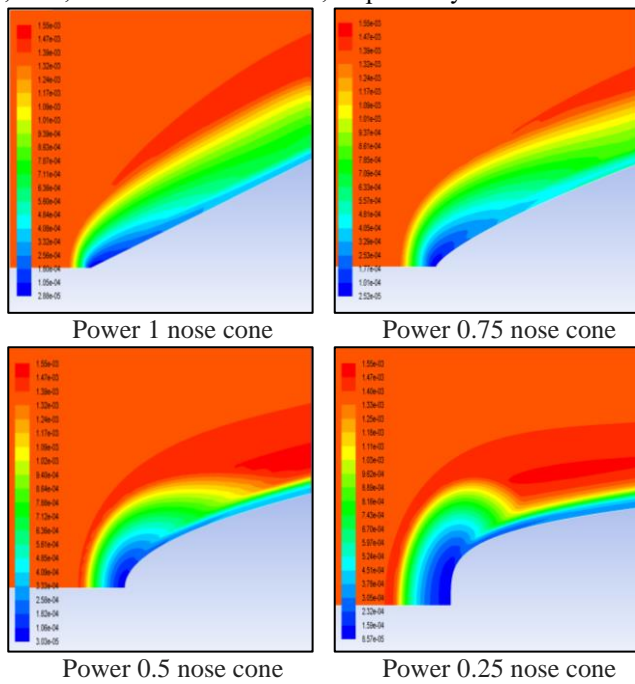


Fig. 22. Turbulence Viscosity Contour of Power Series Nose Cones

d. *Velocity Change Over the Curve Length*

Fig. 23 compares the velocity of the power series nose cone along the curve length. It was observed from the graph that on power 1 nose cone, the velocity at the nose cone tip is high because the shape is conical and as the power of the nose cone decreases, the bluntness of the nose cone increases, this creates a large stagnation on the nose tip, so the velocity is very less in case of power 0.25 nose cone.

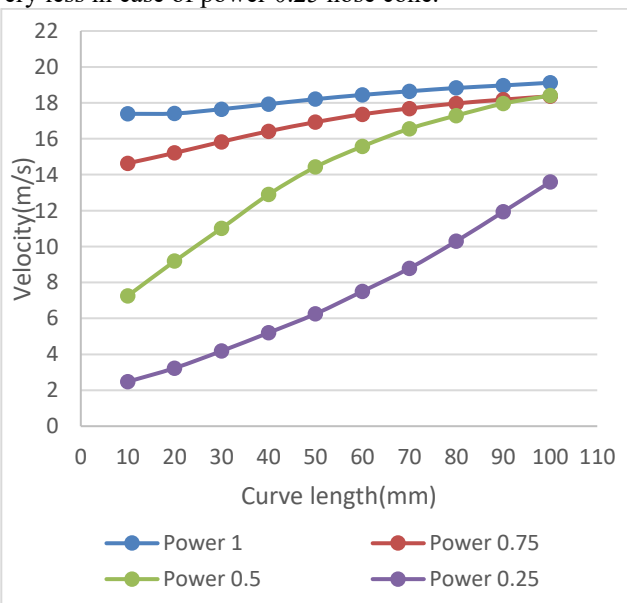


Fig. 23. Velocity Variation for Different Nose Cone Profiles

e. *Drag Coefficient Variation between the K-Sst Model and the Inviscid Model.*

The inviscid flow model and k-SST turbulence model were used for the power series nose cone to find out the

fluctuation in drag coefficient as shown in Fig. 24. As seen in the graph, the values of Cd for every nose cone profile when using the k-SST model are much higher than the values of Cd when using the inviscid turbulence model. In the k-SST turbulent model, the introduction of skin friction drag causes this phenomenon. Because of its blunted form, which reduces the amount of surface area as compared to a pointed nose cone, the power 0.25 nose cone experiences less Cd than all other power series nose cone profiles in both circumstances, as seen by the graph. Therefore, under these circumstances, the power 0.25 nose cone will have more aerodynamic efficiency than other nose cone profiles.

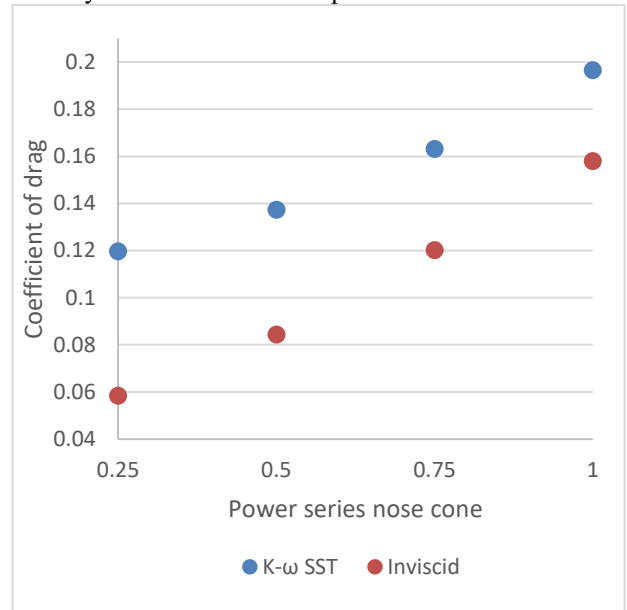


Fig. 24. Drag Coefficient Variation Between The K-Sst Model and the Inviscid Model

B. *Comparison of Experimental and Numerical Outcomes*

Experimental measurements of static pressure and velocity were made, and the findings were compared with numerical data to verify the trend of the graph.

a. *Comparisons of Static Pressure for Power Series Nose Cone*

Fig. 25 shows the comparison of static pressure between CFD and experimental for power series nose cone profile. The static pressure is less in power 1 nose cone as compared to other nose cone profiles and high in power 0.25 nose cone because power 1 nose cone is sharp at the tip, so the stagnation region at the tip is much less as compared to other nose cone profiles. Due to less stagnation occurring, the velocity reduction is much less at the tip, that's why static pressure is less in the power 1 nose cone. The power 0.25 is the most blunted nose cone among the power series nose cones, so the stagnation region at the tip is large, that's why the static pressure is high in the power 0.25 nose cone.

The slope of the static pressure curve in the power 1 nose cone is less because velocity increased at a slow rate, so the static pressure decrement is less.

As we decrease the power of the nose cone, the bluntness of the nose cone increases, and velocity increases, so the slope of static pressure decreases drastically in the case of power 0.25 nose cone.

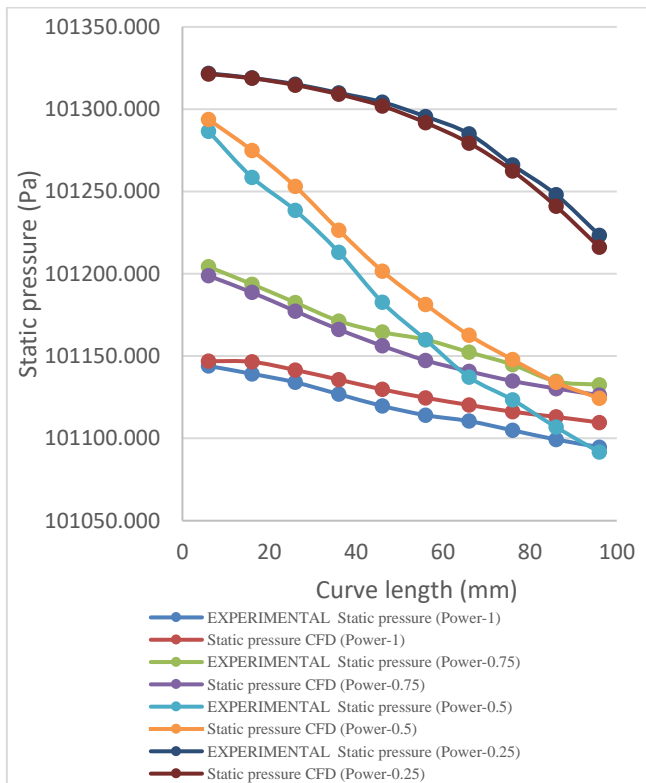


**Fig. 25. Comparison of the Static Pressure of Various Nose Cone Profiles Between CFD and Experimental**

The reason behind the steepness of the power 0.5 nose cone is due to its shape, the acceleration from nose tip to base is large, so the decrement in static pressure is large.

*b. Comparisons of Velocity for Power Series Nose Cone*

Fig. 26 shows the comparison of velocity for all the Power series nose cones between CFD analysis and experimental data. The velocity of power 1 nose cone is the highest amongst all the other nose cone profiles because it is sharp at the leading edge, so the stagnation occurred less at the nose tip hence the reduction of free stream velocity is much less. As we reduce the power of the nose cone, the nature of the curve changes from sharpness to bluntness. As the 0.25 power nose cone is the bluntest, it creates a very large amount of stagnation, hence velocity is very low on this cone at the leading edge of the cone. The slope of the velocity curve in the power 1 nose cone increases gradually because of its conical shape, the stagnation that occurs is much less and the static pressure decreases at a very slow rate and vice versa for the power 0.25 nose cone.

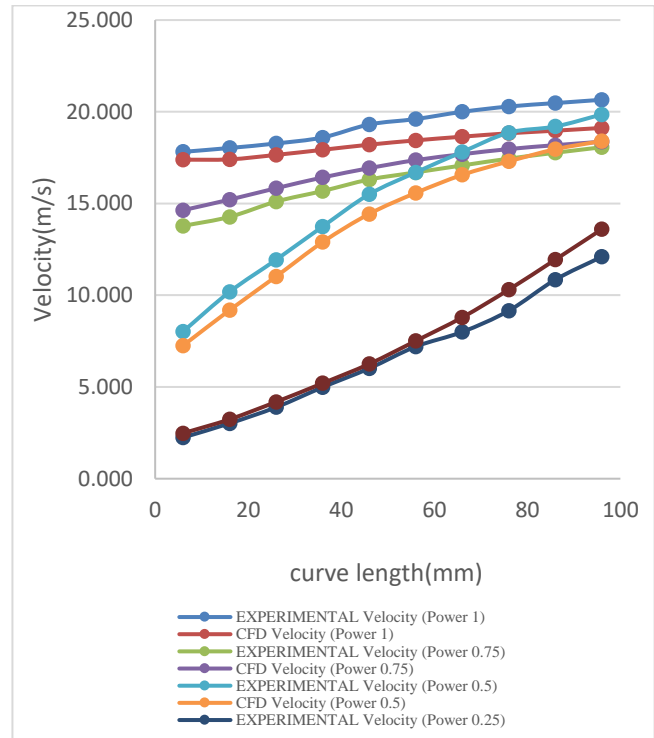


**Fig. 26. Comparison of the Velocity of Various Nose Cone Profiles Between CFD and Experimental**

**IV. CONCLUSION**

In this study, the aerodynamic performance of various nose cones was examined using both computational and experimental methods. All the nose cone profiles with the same L/D ratio were investigated at zero angle of attack with a velocity of 25 m/s. The experimental data of pressure and velocity was compared with computational data to verify the trend of the graph obtained by experiments. The primary factor in choosing the best shape for the subsonic flow range among all the power series nose cone profiles was the drag coefficient. The following are the conclusions of the entire study carried out in this project:

- 1) The trailing edge velocity for power 1, 0.75, 0.5 and 0.25 was determined to be 17.388 m/s, 14.637 m/s, 7.255 m/s and 2.477 m/s respectively.
- 2) The highest-pressure coefficient was found at the nose tip whereas the highest dynamic pressure is at the trailing edge for all nose cone profiles investigated.
- 3) The drag coefficient experienced by power 1, 0.75, 0.5 and 0.25 nose cones are 0.197, 0.163, 0.137 and 0.12 respectively.
- 4) The skin friction drag coefficient for power 1, 0.75, 0.5 and 0.25 was found to be 0.0387, 0.043, 0.053, and 0.061, respectively.
- 5) It is also concluded that the power 0.25 nose cone has more skin friction drag due to its more surface area as compared to other nose cone profiles, but the overall coefficient of drag is the least among all other nose cone profiles. So, the power 0.25 nose cone has the best aerodynamic performance among all the nose cones tested.

# Experimental and Numerical Analysis Over Power Series Nose Cone

This study can be used for further calculation and testing of power series nose cones and 0.25 power nose cones can be used in subsonic vehicles as it gives the least drag at subsonic speed. Further testing for power series nose cones can be done for different Mach numbers.

## DECLARATION STATEMENT

Funding	No, I did not receive.
Conflicts of Interest	No conflicts of interest to the best of our knowledge.
Ethical Approval and Consent to Participate	No, the article does not require ethical approval and consent to participate with evidence.
Availability of Data and Material/ Data Access Statement	Not relevant.
Authors Contributions	I am only the sole author of the article

## REFERENCES

1. Anderson J.D., "Fundamentals of Aerodynamics", McGraw-Hill, New York, NY, USA, 2007.
2. Subha, Rosy & D'rozario, Anthony Mario & Manojith, Sreeshin, "Study on Various Types of Nose Cone Profiles at Supersonic Speed Through Analytical", Experimental And Numerical Simulation Methods. Journal of Xidian University. 14. 10.37896/Jxu14.6/312, 2020. <https://doi.org/10.37896/jxu14.6/312>
3. Yeshwanth, A. & Senthil, P.V. "Nose cone design and analysis of an avion", International Journal of Pure and Applied Mathematics, 119. 15581-15588, 2018.
4. Kumar, P. Kiran. "Analysis of nose cone of the missile." International Journal of Engineering Research and Applications, ISSN 2248-9622, 2020.
5. Rozario and Anthony Mario, "Study on Various Types of Nose Cone Profiles at Supersonic Speed through Analytical, Experimental and Numerical Simulation Methods."
6. Schinetsky P. A., B. T. Brooker, A. Treadway, S. M. Olcmen, S. E. Jones, "Numerical and experimental analysis of projectile nose geometry", Journal of Spacecraft and Rockets, 52(5), 1515-1519, 2015. <https://doi.org/10.2514/1.A33316>
7. Foster N. F., G. S. Dulikravich, "Three-dimensional aerodynamic shape optimization Using genetic and gradient search algorithms," Journal of Rockets and Spacecraft, 34(1), 36-42, 1997. <https://doi.org/10.2514/2.3189>
8. Deepak N. R., T. Ray, R. R. Russell, "Evolutionary algorithm Shape Optimization of a Hypersonic Flight Experiment Nose Cone", Journal of Spacecraft and Rockets, 45(3), 2008. <https://doi.org/10.2514/1.33826>
9. Ranjan R. R., D. V. Parmar, H. K. Raipuria, P. B. Singh, "Innovative nose cone design of aircraft", ASME International Mechanical Engineering Congress and Exposition, Texas, USA, November 2015. <https://doi.org/10.1115/IMECE2015-50264>
10. Garry A., Crowell Sr, "The Descriptive Geometry of Nose Cone", 1996.
11. Varma A. S., G. S. Sathyanarayana, "CFD analysis of various nose profiles", International Journal of Aerospace and Mechanical Engineering, 3(3), 26-29, 2016.
12. Harish S., D. Hasen, V. Giridharan, "Computational study on surface pressure distribution and base pressure distribution over parabolic series nose cone", Journal of Chemical and Pharmaceutical Sciences, 9(2), 0974-2115, 2016.
13. Rafie, A. S. M., Magaidi, A. M., & Marzuki, O. F. (2019). Aerodynamic Performance of Biomimicry Snake-Shaped Airfoil. In International Journal of Engineering and Advanced Technology (Vol. 9, Issue 2, pp. 3319-3323). <https://doi.org/10.35940/ijeat.b3560.129219>
14. Mishra, N. K., Kumar, A. S., Ganesh, M., & Rehman Alam, M. A. (2019). Design of Minimum Length Supersonic Nozzle using the Method of Characteristics. In International Journal of Innovative Technology and Exploring Engineering (Vol. 9, Issue 2, pp. 1370-1374). <https://doi.org/10.35940/ijitee.b6183.129219>
15. P. D., Verma, A., Reddy, C. J., Suri S. J., & M, V. (2020). Boundary Layer Control of Airfoil using Rotating Cylinder. In International Journal of Recent Technology and Engineering (IJRTE) (Vol. 8, Issue 6, pp. 4742-4750). <https://doi.org/10.35940/ijrte.e9862.038620>
16. Shaheen, A., & Sinha, A. D. (2020). Crash Analysis of Aircraft Nose Prototype. In International Journal of Engineering and Advanced Technology (Vol. 9, Issue 6, pp. 204-213).

17. Pandey, S., & Samanta, A. (2020). Real-time Forecasting of COVID-19 Prevalence in India using ARIMA Model. In International Journal of Management and Humanities (Vol. 4, Issue 10, pp. 78-83). <https://doi.org/10.35940/ijmh.j0973.0641020>

## AUTHOR PROFILE



Propulsion, JRF

Mr. Vineet Kumar Rathi is the sole author of this research. Presently serving as a Junior Research Fellow at IIT Goa, he is actively involved in diverse combustion research. With a notable portfolio in the aerospace sector, he has undertaken numerous projects. His primary focus revolves around the aerodynamics and propulsion of aerospace vehicles. B. Tech Aerospace, M. Tech Rocket

**Disclaimer/Publisher's Note:** The statements, opinions and data contained in all publications are solely those of the individual author(s) and contributor(s) and not of the Blue Eyes Intelligence Engineering and Sciences Publication (BEIESP)/ journal and/or the editor(s). The Blue Eyes Intelligence Engineering and Sciences Publication (BEIESP) and/or the editor(s) disclaim responsibility for any injury to people or property resulting from any ideas, methods, instructions or products referred to in the content.